Squaric acid adsorption and oxidation at gold and platinum electrodes

William Cheuquepán, Jorge Martínez-Olivares, Antonio Rodes, José Manuel Orts

PII: S1572-6657(17)30725-7
DOI: doi:10.1016/j.jelechem.2017.10.023
Reference: JEAC 3583

To appear in: *Journal of Electroanalytical Chemistry*

Received date: 28 July 2017
Revised date: 6 October 2017
Accepted date: 10 October 2017

Please cite this article as: William Cheuquepán, Jorge Martínez-Olivares, Antonio Rodes, José Manuel Orts , Squaric acid adsorption and oxidation at gold and platinum electrodes. The address for the corresponding author was captured as affiliation for all authors. Please check if appropriate. Jeac(2017), doi:10.1016/j.jelechem.2017.10.023

Squaric acid adsorption and oxidation at gold and platinum electrodes

William Cheuquepán[b], Jorge Martínez-Olivares, Antonio Rodes[a,b,*], José Manuel Orts[a,b]

[a] Departamento de Química Física and [b] Instituto Universitario de Electroquímica

Universidad de Alicante

Apartado 99, E-03080 Alicante, Spain

*Corresponding author

E-mail: Antonio.Rodes@ua.es

Phone and fax: 965909814

Abstract

The adsorption and oxidation of squaric acid (3,4-dihydroxycyclobut-3-ene-1,2-dione, $H_2C_4O_4$, SQA) at platinum and gold electrodes were studied spectroelectrochemically in perchloric acid solutions. Voltammetric experiments demonstrate that reversible adsorption takes place at gold electrodes in the double-layer region. As a difference with platinum electrodes, no dissociative adsorption processes leading to the blocking of the electrode surface are detected. ATR-SEIRAS experiments show potential-dependent adsorbate bands at potentials below 1.20 V RHE that, according to DFT calculations, can be assigned to adsorbed squarate. For platinum electrodes, the potential-dependent adsorption of squarate anions is coupled with the oxidative stripping of adsorbed carbon monoxide, which is formed upon dissociative SQA adsorption. Bonding of squarate species to the platinum and gold surfaces involves two oxygen atoms in a bidentate configuration, with the molecular plane perpendicular to the metal surface. The ATR-SEIRA spectra obtained for gold electrodes in the SQA oxidation region show bands for adsorbed bicarbonate anions formed from dissolved carbon dioxide molecules. In the case of platinum, distinct bands are observed for adsorbed oxidation products which probably are formed upon opening of the SQA ring.

Keywords: squaric acid; squarate anions; platinum; gold; thin film electrodes; ATR-SEIRAS; DFT

1. Introduction

Oxocarbons, such as squaric (3,4-dihydroxycyclobut-3-ene-1,2-dione, $H_2C_4O_4$, SQA), croconic ($H_2C_5O_5$) and rhodizonic ($H_2C_6O_6$) acids, are small cyclic organic compounds with relatively high acid dissociation constant values. The latter are related to a remarkable stability of their anions due to electronic π-delocalization [1, 2]. As a typical characteristic of neutral oxocarbon molecules [3], strong hydrogen bonds determine the structures of squaric acid both in solid crystals [4] and in adsorbed phases [5]. In recent years, squaric acid and its derivatives have been the object of studies dealing with a variety of properties of these compounds. For instance, derivatives of squaric acid are versatile synthons that have been envisaged as bioisosteric replacements for various functional groups in bioorganic and medicinal chemistry [6]. In this context, the pharmaceutical applications of squaric acid (di)esters and (di)amides have been described [7, 8]. Moreover, condensation of squaric acid with electron-rich aromatic rings gives rise to squaraines dyes, which are interesting fluorophore compounds [9, 10] that can be used either in solution [11] or forming a self-assembled monolayer [12]. Again, hydrogen bonding seems to play a key role in the aggregation of squaraine molecules, which determines the photochemical properties of these compounds [13]. Squarate anions have also been used in the synthesis of metal nanoparticles [14, 15], either as a reducing and stabilizing agent in the case of gold [14] or as a surfactant that favours the formation of cubic platinum nanoparticles as a result of facet-selective adsorption [15]. Squaric acid has also been employed for obtaining 3D cube-shaped composites and porous carbon microparticles [16]. Recently, the fabrication of porous alumina upon anodization in squaric acid solutions has been described [17]. Finally, squaric acid has been used for the development of different kinds of biosensors [18, 19].

Some papers have been published on the electrochemical reactivity of squaric acid [20] and some of its derivatives [21] in non-aqueous solvents. Oxidation of squarate anions at platinum electrodes proceeds through consecutive reversible monoelectronic transfer processes involving anion radical species [20]. Sazou and Kokkinidis [22] studied the electrochemical oxidation of SQA in aqueous solutions on platinum and adatom-modified platinum electrodes. The authors reported the isolation of the hydrated form of cyclobutantetrone (CBT) as the overall product of SQA oxidation and proposed the existence of adsorbed (and discharged) hydrogensquarate and squarate anions as intermediate species [22]. It was proved later that the electrochemical behaviour of oxocarbons at platinum electrodes is characterized by parallel reaction paths involving, in addition to their direct oxidation at potentials close to the

onset of the electrode oxidation reaction, an effective blocking of the electrode surface for the hydrogen adsorption-desorption processes [23-29]. In contrast with the stability of squaric acid and hydrogensquarate anions in solution, the observed surface blockage of platinum electrodes in SQA-containing solutions is related to the dissociative adsorption of SQA to form adsorbed carbon monoxide. This adsorbate has been identified from the in situ IRRAS (InfraRed Reflection Absorption Spectroscopy) data collected with polycrystalline [24] and single crystal [28] platinum electrodes. Similar behavior has been reported for other oxocarbons such as croconic [25, 26] and rhodizonic [27] acids. The effect of adsorbed adatoms on the electrochemical behavior of oxocarbons on platinum electrodes has also been studied [30].

As described above, CO formation and its subsequent oxidation dominate the electrochemical behavior of platinum electrodes in the presence of oxocarbons. In the case of squaric acid, the formation of adsorbates different from CO has been detected and the formed adspecies tentatively identified as adsorbed squarate anions [28]. This adsorption process takes place in a narrow potential window located between the onset of the oxidative stripping of the CO adlayer and that for the oxidation of the aforementioned adsorbed species [28]. Due to the weak adsorption of carbon monoxide on gold [31, 32], a non-significant blockage of gold electrodes could be expected in SQA-containing solutions. In this way, an in situ SERS (Surface Enhanced Raman Spectroscopy) study of SQA adsorption at polycrystalline gold electrodes [33] showed a residual carbon monoxide band only after long exposures of the electrode to the SQA solution. Other than the band for adsorbed CO, a variety of adsorbate features was reported in the SERS spectra that were assigned to different moieties of squaric acid and hydrogensquarate species bonded either through their hydroxyl or through their carbonyl groups depending on the presence or the absence of coadsorbed chloride anions [33].

In this work we present new spectroelectrochemical results regarding the adsorption and reactivity of squaric acid at gold and platinum thin film electrodes. ATR-SEIRAS (Surface Enhanced Infrared Reflection Absorption Spectroscopy under Attenuated Total Reflection conditions) experiments carried out with the so-called Kretschmann's configuration have provided additional data on the nature of the adsorbed species formed from SQA thanks to the improved sensitivity associated to the SEIRA effect and the decreased interferences from dissolved species, including the solvent. A preliminary DFT (Density Functional Density) study is carried out to obtain optimized geometries and vibrational frequencies for squarate adsorbed at platinum and gold (111) surfaces providing a basis for the interpretation of the experimental

spectra that could confirm previous assignments for the adsorbate bands observed for platinum electrodes in SQA-containing solutions.

2. **Experimental**

Working solutions were prepared from solid SQA (99% Acros Organics), concentrated perchloric acid (Merck Suprapur®) and ultrapure water (18.2 MΩ·cm, TOC 50 ppb max, Elga Vivendi). These solutions were deaerated with Ar (N50, Air Liquide) and blanketed with this gas during the experiments.

All the voltammetric and in situ infrared experiments were performed in glass cells using a reversible hydrogen electrode (RHE) as the reference electrode and a gold wire as the counter electrode. The polyoriented quasi-spherical gold and platinum beads used as working electrodes in most of the voltammetric experiments were prepared by melting 99.9995% gold (Alfa-Aesar) and platinum (Goodfellow) wires. Some voltammetric experiments were carried out with Au(111) and Au(100) single crystals prepared by using Clavilier's method [34, 35]. Prior to each experiment, platinum [36] and gold [35, 37, 38] electrodes were flame-annealed, cooled down in air and protected with a droplet of ultrapure water. Gold and platinum thin films used as working electrode in the internal reflection infrared spectroscopy experiments were deposited on one of the faces of a low oxygen-content silicon prism beveled at 60^{o} (Pastec Ltd, Japan). Deposition of a 25 nm-thick gold thin film (99.999%, Kurt J. Lesker Ltd.) was carried out by thermal evaporation in the vacuum chamber of a PVD75 (Kurt J. Lesker Ltd.) coating system at a base pressure around 10^{-6} Torr. The thickness of the gold film and the deposition rate (fixed at 0.006 nm s^{-1}) were controlled with a quartz crystal microbalance. In the case of platinum, thin film electrodes were chemically deposited following the procedure described by Silva et al [39]. Once in the spectroelectrochemical cell, the gold and platinum thin film electrodes were cleaned by applying a few voltammetric cycles up to 1.70 V in the 0.1 M $HClO_4$ solution.

In situ infrared experiments were carried out with a Nexus 8700 (Thermo Scientific) spectrometer equipped with a MCT-A detector and a wire grid ZnSe polarizer (Pike Tech). The spectroelectrochemical cell [40, 41] was placed at the top of a Veemax (Pike Tech.) reflectance accessory. All the spectra were collected with a resolution of 8 cm^{-1} and are presented in

absorbance units (a.u.) as $-\log(R/R_o)$, where R and R_o represent the single beam sample and reference reflectivity spectra, respectively. Thus, positive-going and negative-going bands correspond, respectively, to gain or loss of species in the sample spectrum with respect to the reference spectrum. The spectra were collected in a rapid scan mode while the electrode potential was swept at 2 $mV \cdot s^{-1}$. In these experiments, each spectrum was the average of a set of 104 interferograms which were collected in ten seconds, thus corresponding to a 20 mV interval. Each spectrum is referred to the reference single beam spectrum collected in the SQA-containing solutions at 0.10 V.

3. Computational details

Optimized adsorption geometries and harmonic vibrational frequencies of squarate anion at Au(111) and Pt(111) surfaces were obtained from DFT calculations using the Vienna Ab-Initio Simulation Program (VASP, v 4.6) [42-45]. All the calculations were carried out using the Projector-Augmented Wave (PAW) method [46] with the pseudopotentials of Kresse and Joubert [47], and a cutoff energy of 400 eV for the plane wave basis set. The functional of Perdew, Burke and Ernzehof [48, 49] was used for treating exchange and correlation interactions.

The slabs used to model the Au(111) and Pt(111) surfaces consisted of four layers (9 gold atoms each) with (3x3) surface periodicity. Optimized geometries of the adsorbates were obtained by allowing the relaxation of the positions of the light atoms. No relaxation of the metal was allowed. The positions of the metal atoms were fixed with the bulk symmetry, and with metal-metal distances of 0.29520 nm and 0.28171 nm for Au and Pt respectively, obtained from the fits to Murnaghan equations of state using the same PBE functional. The surfaces of neighbouring slab replicas were separated by a vacuum region of more than 12 Angstrom.

Smearing was accomplished with the order-2 Methfessel-Paxton method [50] (with sigma=0.2 eV). K-points sets for sampling of the Brillouin zone were generated using the automatic Monkhorst-Pack [51] method, with a gamma-centered (5 x 5 x 1) scheme. The convergence criteria were: changes in energy smaller than 10^{-5} eV for the electronic step, and Hellman-Feynman forces on atoms below 0.02 eV/Angstrom for the geometry optimization.

Harmonic vibrational frequencies were calculated in the harmonic approximation from the energies corresponding to displacements of +/-0.015 Angstrom in each spatial coordinate of the optimized adsorption geometries. The main contributions to the normal modes corresponding to the calculated vibrational frequencies were visualized using Jmol [52]. The calculated frequencies are reported without any scaling correction. From similar studies in previous work, the relative error (in average) of the calculated frequencies can be estimated to be below 2-3% of the theoretical frequency value.

4. Experimental results

4.1. Voltammetric results

The inset in Figure 1 shows consecutive cyclic voltammograms recorded for a polyoriented platinum electrode, after immersion at 0.10 V in a 10^{-5} M SQA + 0.1 M $HClO_4$ solution, in the potential range corresponding to the hydrogen adsorption-desorption region (curves b). As described in previous papers [23, 24, 28], and in contrast with the behavior of the platinum electrode in the SQA-free solution (curve a1), no defined peaks appear for hydrogen adsorption/desorption at (110) and (100) sites. Decreasing charge densities are observed for hydrogen adsorption with cycling due to the blocking of the adsorption sites by strongly adsorbed species coming from SQA. These species, which have been previously identified as adsorbed CO [24, 28], are already formed at the immersion potential and their coverage increases with cycling. Once a stationary cyclic voltammogram is obtained in the potential region between 0.06 and 0.40 V (curve c1), the potential excursion was extended up to 1.70 V (curve c2). Irreversible oxidation peaks appear in the potential range 0.65-0.85 V, which is typical for the oxidative stripping of adsorbed carbon monoxide [53, 54], followed by a wide oxidation peak at around 1.15 V. This latter feature is superimposed to the currents associated to the oxidation of the platinum electrode surface (see curve a2 for the SQA-free solution).

Experiments carried out in solutions containing SQA with concentrations up to 10 mM are shown in Figure 2. The blocking of the hydrogen adsorption sites observed in the stationary voltammogram between 0.05 and 0.40 V becomes higher as the SQA concentration increases (see inset in Figure 2). At the same time, the oxidation peaks in the potential region between 0.6 and 1.0 V are shifted to more positive potentials and the corresponding charge density

increases with a sub-linear dependence with SQA concentration, suggesting the existence of a saturation value. This behavior is typical of the irreversible oxidation of (sub)monolayers of strongly adsorbed species which is the case for adsorbed carbon monoxide. The oxidation peak potential and its fine structure are related to the effect of adsorbate coverage and adlayer structure, which determines lateral interaction between adsorbed CO molecules and interfacial water (or OH) within the adlayer, and the existence of a distribution of adsorption sites with different energetics [55, 56]. The oxidation peak at potentials above 1.0 V increases clearly with SQA concentration, suggesting that it corresponds mainly to the oxidation of dissolved SQA (or hydrogensquarate) species. Taking into account the pKa values for SQA (0.54 and 3.48 [19]), the latter species predominate in the working solution with a pH value around 1.0. The shape of the corresponding voltammetric peaks indicates a strong effect of adsorption on the SQA oxidation reaction.

Cyclic voltammetry experiments were carried out with polyoriented gold electrodes in perchloric acid solutions containing SQA concentrations up to 10 mM. In the double layer region (Figure 3A), stationary voltammograms are reached from the second voltammetric cycle that show an excess of charge density for increasing SQA concentrations. As the onset of SQA oxidation (see below) is shifted to less positive potentials with increasing SQA concentrations, the upper potential limit in these experiments has been lowered accordingly in order to avoid significant SQA oxidation. Under these conditions, the stability of the voltammetric curves suggests the existence of reversible adsorption/desorption processes of species coming from SQA. Two broad features appear in the cyclic voltammograms reported in Figure 3A between 0.05 and 0.50 V and between 0.50 and 0.90-1.0 V, both shifting to less positive potentials as SQA concentration increases. Besides, a small feature is observed at ca. 0.83 V in the 10 mM SQA solution. A similar but more intense peak appears at the same potential in the cyclic voltammogram recorded for a Au(111) electrode in the same solution (see Figure 3B). Thus, the spike in Figure 3A can be related to the adsorption of species coming from SQA at the (111)-oriented facets of the polyoriented bead electrode. This voltammetric feature is similar to that reported in sulphuric acid solutions for (111) domains and ascribed to an order-disorder transition within the sulfate adlayer [57]. Similar features are also observed for other molecules such as cyanuric acid [58]. Note that no voltammetric peak appears at 0.83 V for Au(100) electrodes in SQA-containing solutions (see also Figure 3B). For this orientation, and similarly to other specifically adsorbed species, differences in the intensity of a voltammetric peak at ca. 0.63 V as recorded during the first and second positive-going sweeps (not shown)

can be associated to an adsorbate-induced lift of the reconstructed surface of the flame-annealed Au(100) electrode [37, 38].

As in the experiments reported above for platinum electrodes, cyclic voltammograms were also recorded after increasing the upper potential limit above 0.90-1.0 V (see Figure 4). Voltammetric profiles showing the existence of irreversible oxidation processes can be observed in the first potential excursion at potentials up to 1.70 V. As a difference with the voltammetric behavior reported for platinum electrodes [23, 24, 28], no oxidation peak appears in the range 0.8-1.0V that could be related to the oxidation of adsorbed CO. Instead, two oxidation peaks can be observed centered at ca. 1.12-1.18 V and 1.40 V, respectively. This latter contribution, which prevails for the higher SQA concentrations, overlaps with the currents due to the oxidation of the gold surface. An inhibiting effect of gold surface oxide on the kinetics of the SQA oxidation reaction could be at the origin of the decreasing currents at potentials around 1.60 V. In the negative-going sweep a small oxidation peak is observed at ca. 1.15 V, i.e. once the surface gold oxide is electrochemically reduced.

4.2. ATR-SEIRAS results

ATR-SEIRAS experiments have been carried out in a 1 mM SQA + 0.1 M $HClO_4$ solution with platinum (Figure 5) and gold (Figure 6) thin film electrodes. In agreement with the surface specificity of the SEIRA effect [59, 60] the bands appearing in the potential-dependent spectra are expected to correspond to adsorbed species being formed/consumed at the electrode surface. In comparison with IRRAS experiments carried out with a thin layer configuration, additional advantages of the internal reflection experiments are related to the lack of potential-dependent signals coming from dissolved species (including bulk water molecules) that could interfere with adsorbate bands. This kind of interference situation was found in previous external reflection infrared experiments performed in SQA-containing solutions with polycrystalline [24] and single crystal [28] platinum electrodes. In these cases, the reported spectra were dominated by consumption bands from squaric acid and (hydrogen)squarate species in solution together with bands related to adsorbed carbon monoxide generated upon the dissociative adsorption of SQA [24, 28]. Additional bands were also observed, in a very narrow potential range and with a relatively low signal-to-noise ratio, at ca. 1784 and 1573 cm^{-1}. These bands can be related to non-dissociated adsorbates coming from SQA [28].

We will present first the potential-difference ATR-SEIRA spectra collected for the platinum thin film electrode. These spectra, shown in Figure 5, are referred to the single beam spectrum collected at 0.10 V in the same solution. As previously reported from external reflection experiments [24, 28], SQA already adsorbs dissociatively at this potential, giving rise to an electrode surface partially covered by adsorbed CO. Thus, all the spectra reported in Figure 5 show a negative-going band at ca. 2055 cm^{-1} corresponding to linearly bonded CO molecules formed at the reference potential. Increasing the electrode potential up to 0.70 V (i.e. the upper limit of the stability range of an almost saturated CO adlayer at platinum electrodes [53, 54]) gives rise to the observation of a positive-going C-O stretching contribution overlapped with the aforementioned negative-going band. The asymmetric bipolar shape of the resulting feature is related to an increase of the CO coverage and the corresponding blue-shift of the C-O stretching band as the electrode potential increases. A less intense bipolar feature appears at ca. 1879 cm^{-1} for bridge-bonded CO [61, 62]. In the potential range between 0.70 and 0.90 V, the intensity of the positive-going lobe of the linearly-bonded CO bipolar feature decreases and new features appear in the spectra at ca. 1760-1775 and 1490-1550 cm^{-1}. These features, whose band frequency values are plotted in Figure 7A, are observed in the spectra recorded between 0.70 and 1.20 V, reaching a maximum integrated band intensity value for potentials around 0.90 V (see Figure 7B). As shown in Figure 7A, a remarkable characteristic of the band at ca. 1500-1550 cm^{-1} is its higher tuning-rate for its potential-dependent frequency value when compared to that at 1760-1775 cm^{-1}. Note also that these spectral features appear at similar frequency values and in a similar potential range as those observed in external reflection spectra for Pt(111) electrodes [28] but now with a much better signal-to-noise ratio.

The spectra collected at potentials higher than 1.20 V show no bands at 1760-1775 and 1490-1550 cm^{-1}. The absence of these features between 1.20 and 1.60 V (see Figure 7B) is parallel to the development of an oxidation peak for platinum electrodes in the SQA-containing solutions for potentials around 1.20 V (see Figure 2). The disappearance of the bands at 1760-1775 and 1490-1550 cm^{-1} takes place together with the development of new spectral features at ca. 1360 and 1720 cm^{-1}, which remain in the ATR-SEIRA spectra for potentials up to 1.60 V (see the corresponding plots in Figure 7A and B).

In the potential-dependent ATR-SEIRA spectra collected with a gold thin film electrode in a 1 mM SQA + 0.1 M $HClO_4$ solution (Figure 6) no features related to adsorbed CO are observed. Instead, the spectra collected for potentials between 0.30 and 1.10 V, show positive-going bands at 1490-1550 and 1760-1775 cm^{-1} for adsorbates being formed from SQA accompanied

by negative-going bands at 3500 and 1610 cm^{-1} corresponding to displaced water molecules. The intensity of the adsorbate bands at 1490-1550 and 1760-1775 cm^{-1} steadily increases with the electrode potential up to 1.10 V (Figure 7B), with the band frequency being shifted to higher wavenumbers (see Figure 7A). As described above for the platinum electrodes, the tuning rate for the band at 1490-1550 cm^{-1} is higher than that for the feature at 1760-1775 cm^{-1}. At 1.30 V, the bands at 1490-1550 and 1760-1775 cm^{-1} disappear and another positive-going feature develops at 1100 cm^{-1} corresponding to adsorbed perchlorate anions [63]. Note that the spectrum obtained at 1.30 V is similar to that observed in SQA-free perchloric acid solutions, including the positive-going feature at ca. 3610 cm^{-1}, which was related to the (O-H) stretching modes for asymmetrically hydrogen-bonded water molecules interacting with adsorbed perchlorate anion [63]. On the other hand, the absence of perchlorate features at potentials below 1.30 V indicates the competitive adsorption between this latter species and those coming from SQA. The oxidative removal of the species related to the bands at 1490-1550 and 1760-1775 cm^{-1} allows the adsorption of perchlorate anions.

The spectra collected at potentials above 1.30 V show decreasing perchlorate bands as expected from the competitive adsorption of oxygenated species formed during the oxidation of the gold surface. When comparing the ATR-SEIRA spectra obtained for gold and platinum electrodes for potentials above 1.20 V, it has to be remarked that no spectral features at ca. 1360 and 1720 cm^{-1} are observed in the case of gold. Instead, an additional absorption band can be observed at ca. 1411 cm^{-1} in the spectra collected at 1.40 V. This feature can be related to the C-OH stretching mode for adsorbed bicarbonate anions [64, 65]. Bicarbonate features can be observed at gold electrodes in the presence of dissolved carbon dioxide either bubbled in the working solution [65] or formed upon the oxidation of carbon-containing species such as oxalic acid [66] or SQA (this work). The direct detection of dissolved CO_2 from the ATR-SEIRA spectra is difficult with the Kretschmann's configuration employed in this work (the produced molecules are not retained close to the electrode surface as in external reflection experiments). Despite of this difficulty, a small feature at 2344 cm^{-1} for dissolved carbon dioxide can be observed by enlarging the spectra collected for potentials above 1.20 V. This feature is more clearly appreciated in the spectra collected at the same potential in a 10 mM SQA solution (not shown).

5. DFT results and discussion

DFT calculations have been carried out with the aim of assigning the observed features in the ATR-SEIRA spectra (other than those corresponding to adsorbed CO in the case of platinum electrodes) to species coming from SQA. In this paper, we focus on the verification of previous tentative assignments to adsorbed squarate anions [28]. Figure 8 shows the optimized adsorption geometries found for the squarate adsorbate on the surfaces of Au(111)-(3x3) and Pt(111)-(3x3) slabs composed of four metallic layers. Different initial positions and orientations of the squarate moiety were tested, all of them leading, as local energy minima, to structures with bidentate bonding to the metal surface. The bonding involves two oxygen atoms that were located approximately at on-top positions nearly above two nearest-neighbour surface metal atoms (the metal-oxygen bonds are slightly tilted from the surface normal: around 6º for the Pt surface, and less than 5º for Au). It must be remarked that the interaction with the surfaces causes significant distortion of the molecular geometry of the free squarate anion, with lose of its fourfold symmetry. This is evidenced by the changes in the C-C and C-O distances that are no longer equivalent in the optimized adsorption geometry. The C-O, C-C and O-metal bond lengths corresponding to the optimized geometries of squarate adsorbed on Pt(111) and Au(111) surfaces are presented in Table 1.

Two slightly different metal-oxygen distances are found in each of the two geometries. The relevant point is that, despite the smaller metallic radius of the platinum atoms as compared to that of gold, the Pt-O distance is significantly shorter (around 216 pm) than the Au-O distances (around 240 pm). This clearly indicates a stronger bond of the squarate adsorbate on the Pt(111) surface.

On both surfaces, three different C-C bond length values can be distinguished. The longer value is found for the C-C bond that joins the carbon atoms farther from the metal. This value (156 and 157 pm, depending on the metal) agrees well with a single C-C bond. The C-C bonds that are essentially normal to the surface have lengths of 151 and 150 pm on Au and Pt, respectively. These shorter distances indicate an increased bond order. The shorter bond length is found for the CC bond that is parallel and closer to the metal surface. For both metals the values are around 145 pm, a value that is intermediate between those characteristic for the C-C single bond (around 154 pm [67]) and those of the C=C double bond (around 134 pm [67]). The distortion of the square ring with loss of symmetry clearly indicates that bonding to the metal affects significantly to the electronic structure of the adsorbed species.

The C-O distances corresponding to the atoms farther from the surface are the same (121 pm) for both metal surfaces, and this bond length agrees well with those tabulated as characteristic of the carbonyl group. On the other hand, the C-Oad distance is slightly longer (126 pm) on the Pt surface than on Au (124 pm).

As described above, the main experimental bands observed for platinum and gold electrodes in SQA-containing solutions (other than those for adsorbed CO in the case of platinum) in the potential range prior to significant surface oxidation, appear around 1490-1550 cm^{-1} and 1760-1775 cm^{-1}. The calculated harmonic vibrational frequencies of adsorbed squarate corresponding to the optimized adsorption geometries shown in Figure 8 are summarized in Table 2. Only the main contribution to the vibrational normal mode is given for each vibration. From the calculated values for both metals, the experimental values could both be assigned to symmetrical OCCO vibrational modes of adsorbed squarate. Namely, the features around 1490-1550 and 1760-1775 cm^{-1}, would be related, respectively, to coordinated and uncoordinated oxygen atoms, thus confirming tentative assignments made in previous papers. The frequencies around 1760-1775 cm^{-1} compare well with those of carbonyl groups in a tensioned ring, in agreement with the lengths found for the C-O moieties that are not in direct contact with the metal. On the other hand, the bond lengths in the O-C-C-O frame directly connected to the surface are consistent with the frequency values in the range 1490-1550 cm^{-1} that correspond to normal modes that result from the stretching of C-C and C-O bonds with a strength intermediate between those of double and single bonds.

Regarding the asymmetric OCCO stretchings, those modes are not expected to be detected as a consequence of the surface selection rule [68], as their dynamic dipole moment is essentially parallel to the electrode surface. This explains the absence of any experimental band for these modes, in particular around 1450 cm^{-1} for the platinum samples (as the contribution around 1530 cm^{-1} for the Au(111) surface would be eventually merged with the band expected at 1566 cm^{-1}, which is indeed observed in the ATR-SEIRAS experiment). The calculated band around 1080-1100 cm^{-1} would not be observable, because of the same reason (absence of non-zero component in the normal direction, as this C-C stretch corresponds to the two carbon atoms that are closer to the metal).

In overall, the effect of the nature of the metal on the calculated frequency values is small. In particular, for the frequencies around 1770-1780 cm^{-1}, corresponding to the in- and out-of-phase vibrations of the two carbonyl groups (in the molecular region distant from the metal surface), the differences remain below 5 cm^{-1}. This value is smaller than the experimental

uncertainty for the measured frequencies. Greater differences are found for the OCCO features at lower wavenumbers. In the case of the symmetric OCCO stretch of the molecule half that is closer to the metal, the differences amount to near 40 cm^{-1}. The differences are even greater for the asymmetric OCCO stretch of this part of the adsorbate. An analysis based on these trends of the experimental frequency values for the observed features for platinum and gold electrodes (corresponding, as discussed above, to the symmetric stretching modes) is complicated by the effect of squarate coverages, that could be different for these metals at a given electrode potential, the effect of coadsorption (carbon monoxide, water and/or hydroxyl or perchlorate anions depending on the electrode potential) and that of the electrode potential. The latter effect is higher (higher values of the experimental tuning rate) for the band around 1490-1550 cm^{-1} as observed in Figure 7A. This observation is in agreement with the greater effect expected for the electronic state of the surface (surface charge density, surface energy levels) on the atoms that are closest and directly bonded to the metal. This is also at the origin of the differences found in the geometry of the OCCO frame that acts as a bidentate ligand, while the two carbonyl groups, that are not in direct contact with the metal, have identical structural features on both metal surfaces.

6. Conclusions

A study of the adlayers formed on Au and Pt electrode surfaces in contact with SQA solutions has been carried out. The combination of spectroelectrochemical techniques (ATR-SEIRAS and cyclic voltammetry) and DFT calculations of adsorption geometries and theoretical harmonic frequencies has provided new insight regarding the nature of the species forming the adlayers.

ATR-SEIRAS has allowed the detection of adsorbed squarate species on gold and platinum thin-layer electrodes, in the potential region prior to the oxidation of the metal surfaces. These species are responsible for the experimental bands observed around 1490-1550 cm^{-1} and 1760-1775 cm^{-1}, which, according to DFT calculations, correspond to the symmetric OCCO stretching modes involving, respectively, the uncoordinated and metal-coordinated oxygen atoms of squarate adsorbed in a bidentate configuration. Taking into account that hydrogensquarate anions are the main species coming from SQA in the working solution, it can be concluded that the detected adsorption process involves a deprotonation step that can be formally described as a lowering of the corresponding pKa value. A similar situation was found in the case of acetic [69, 70] and other (di)carboxylic acids [71]. In these latter cases, the pKa of

the uncoordinated carboxylic group seems also to be lowered in comparison to the second pKa for the corresponding dissolved species in an extent that decreases as the size of the molecule increases from (hydrogen)oxalate to (hydrogen)succinate [71]. In other cases, such as bisulfate [72] and mercaptoundecanoic acid [73] higher values of the pKa for the adsorbate in comparison to the dissolved species have been reported. In any case, we do not claim that the results reported here (namely, an apparently increased dissociation constant for the adsorbed hydrogensquarate anion in comparison to the dissolved species) reflect a general trend for all the protonated groups of any adsorbed species. Besides, and even if we can neither completely exclude the presence of adsorbed hydrogensquarate anions or SQA molecules at the electrode surface, we can conclude from the present results that adsorbed squarate is the prevailing adsorbate (other than CO in the case of platinum) coming from SQA. More work is in progress, including ATR-SEIRAS experiments at various SQA concentrations and additional DFT calculations, in order to test the presence of either squaric acid molecules or hydrogensquarate anions at gold electrodes.

ATR-SEIRAS data also reflect the potential-dependent behavior of squarate adsorption with an onset potential that, in the case of platinum electrodes, is determined by the stability of the CO adlayer formed upon SQA dissociative adsorption. At potentials above 0.90 V for platinum and 1.0 V for gold electrodes, adsorbed squarate is oxidatively stripped from the electrode surface leading to a nearly zero surface coverage at ca. 1.20 V. Detected adsorbed species coming from SQA oxidation at gold electrodes are bicarbonate anions, which are formed from dissolved carbon dioxide (this latter species being hardly detected in the ATR-SEIRA spectra). In the case of platinum electrodes, it was clear from previous infrared external reflection data for SQA oxidation that carbon dioxide is produced [24, 28]. Moreover, it has been reported for Pt(111) and Pt(110) electrodes in CO_2-saturated solutions the observation of adsorbate bands at ca. 1500-1550 and 1430-1450 cm^{-1} [64, 74] that were ascribed to adsorbed carbonate and bicarbonate anions, respectively [64]. These bands are not observed in the potential region where carbon dioxide can be generated upon SQA oxidation, thus suggesting that the production of carbon dioxide is higher in the case of gold.

Another distinct feature for the platinum electrodes in the SQA-containing solutions is the observation of adsorbate bands in the ATR-SEIRA spectra at ca. 1720 and 1360 cm^{-1} for potentials between 1.20 and 1.60 V. A detailed discussion of the nature of the species giving rise to these bands is out of the scope of this paper. We can just recall here that CBT was identified by Sazou and Kokkinidis [22] as a product of SQA oxidation on platinum electrodes.

An absorption band around 1740 cm^{-1} in the infrared external reflection spectra obtained for platinum electrodes during SQA oxidation was tentatively related to the formation of CBT [24, 28]. Whether this species can be adsorbed at the platinum electrode is an open question. In any case, it must be taken into account that from the point of view of their elemental composition, squarate and CBT are not distinguishable. They only differ in the total number of electrons. This means that DFT calculations of neutral systems as those carried out in this work do not allow to distinguish between the adsorption of cyclobutantetrone (CBT) and discharged squarate anion. Additionally, other possible oxidation products could be envisaged. For instance, if an oxidative opening of the squaric ring could take place, the possibility of forming diketosuccinic acid or similar species would have to be taken into account, leading to new lines of research. Work is in progress to explore some of these possibilities and gain further insight on the electrochemical behaviour of squaric acid and other oxocarbons.

Acknowledgements.

Prof. Juan M. Feliu is acknowledged for providing the gold single crystal electrodes used in this work. The authors acknowledge the funding by Ministerio de Economía y Competitividad through projects CTQ2016-76221-P (AIE/FEDER, UE) and CTQ2016-76231-C2-2-R (AEI/FEDER, UE) and by the University of Alicante (VIGROB-263).

Figure captions

Figure 1. Cyclic voltammograms obtained for a polyoriented platinum electrode in 0.1 M $HClO_4$ (curves a) and 10^{-5} M SQA + 0.1 M $HClO_4$ (curves b and c) solutions. Curves b in the inset show the first voltammetric cycles recorded in the hydrogen adsorption-desorption region. Curve c1 corresponds to the stationary voltammogram recorded under these latter conditions whereas curve c2 shows the subsequent voltammetric cycle up to 1.60 V. Sweep rate: 50 $mV \cdot s^{-1}$.

Figure 2. Cyclic voltammograms obtained for a polyoriented platinum electrode in a x M SQA + 0.1 M $HClO_4$ solutions. The inset shows the stationary voltammograms recorded in the hydrogen adsorption-desorption region before the subsequent cycles up to 1.60 V. x= a) 0 ; b) 10^{-5} ; c) 10^{-4} ; d) 10^{-3} ; e) 10^{-2} . Sweep rate: 50 $mV \cdot s^{-1}$.

Figure 3. Stationary cyclic voltammograms obtained for A) polyoriented gold and B) Au(111) and Au(100) electrodes in a x M SQA + 0.1 M $HClO_4$ solutions. x= a) 10^{-5}; b) 10^{-4} ; c) 10^{-3} ; d) and B) 10^{-2} ; Sweep rate: 50 $mV \cdot s^{-1}$.

Figure 4. Cyclic voltammograms obtained for a polyoriented gold electrode in a first potential excursion up to 1.70 V in x M SQA + 0.1 M $HClO_4$ solutions. x= A) 10^{-5}; B) 10^{-4}; C) 10^{-3}; D) 10^{-2}. Sweep rate: 50 $mV \cdot s^{-1}$.

Figure 5. Potential-difference ATR-SEIRA spectra collected with a platinum thin film electrode in a 1 mM SQA + 0. 1 M $HClO_4$ solution. The reference spectrum was collected at 0.10 V in the same solution.

Figure 6. Potential-difference ATR-SEIRA spectra collected with a gold thin film electrode in a 1 mM SQA + 0. 1 M $HClO_4$ solution. The reference spectrum was collected at 0.10 V in the same solution.

Figure 7. Potential-dependent band frequencies (A) and integrated band intensities (B) for the bands observed between 1350 and 1800 cm^{-1} in the ATR-SEIRA spectra collected with platinum and gold thin film electrodes in contact with 1 mM SQA + 0.1 M $HClO_4$ solutions. Open and solid symbols correspond to gold and platinum bands, respectively. The same symbol is used in A and B for each observed band.

Figure 8. Optimized adsorption geometries of squarate at A) Au(111) and B) Pt(111). (a-c) C-C bonds for which distances are given in Table 1.

Reference list.

[1] G. Maahs, P. Hegenberg, Syntheses and derivatives of squaric acid, Angew. Chem., 78 (1966) 927-931.
[2] R. West, Ed., Oxocarbons, Academic Press, New York, 1980.
[3] S. Horiuchi, Y. Tokunaga, G. Giovannetti, S. Picozzi, H. Itoh, R. Shimano, R. Kumai, Y. Tokura, Above-room-temperature ferroelectricity in a single-component molecular crystal, Nature 463 (2010) 789-792.
[4] D. Semmingsen, F.J. Hollander, T.F. Koetzle, A neutron diffraction study of squaric acid (3,4-dihydroxy-3-cyclobutene-1,2-dione), J. Chem. Phys., 66 (1977) 4405-4412.
[5] K. Ueji, J. Jung, J. Oh, K. Miyamura, Y. Kim, Thermally activated polymorphic transition from a 1D ribbon to a 2D carpet: squaric acid on Au(111), Chem.Commun., 50 (2014) 11230-11233.
[6] M. Lu, Q.-B. Lu, J.F. Honek, Squarate-based carbocyclic nucleosides: Syntheses, computational analyses and anticancer/antiviral evaluation, Bioorg. Med. Chem. Lett., 27 (2017) 282-287.
[7] N.B. Silverberg, J.K. Lim, A.S. Paller, A.J. Mancini, Squaric acid immunotherapy for warts in children, J. Am. Acad. Dermatol., 42 (2000) 803-808.
[8] P. Freyschmidt-Paul, J.P. Sundberg, R. Happle, K.J. McElwee, S. Metz, D. Boggess, R. Hoffmann, Successful treatment of alopecia areata-like hair loss with the contact sensitizer squaric acid dibutylester (SADBE) in C3H/HeJ Mice, J. Invest. Dermatol., 113 (1999) 61-68.
[9] A. Ajayaghosh, Chemistry of squaraine-derived materials: Near-IR dyes, low band gap systems, and cation sensors, Acc. Chem. Res., 38 (2005) 449-459.
[10] S. Sreejith, P. Carol, P. Chithra, A. Ajayaghosh, Squaraine dyes: a mine of molecular materials, J. Mater. Chem., 18 (2008) 264-274.
[11] P. Marks, M. Levine, Synthesis of a Near-Infrared Emitting Squaraine Dye in an Undergraduate Organic Laboratory, J. Chem. Educ., 89 (2012) 1186-1189.
[12] S.H. Kim, S.K. Han, S.M. Lee, J.H. Im, J.H. Kim, K.N. Koh, S.W. Kang, Preparation and spectroscopic characterization of a self-assembled monolayer of squarylium dye on gold, Dyes Pigm., 45 (2000) 23-28.
[13] K.T. Arun, B. Epe, D. Ramaiah, Aggregation behavior of halogenated squaraine dyes in buffer, electrolytes, organized media, and DNA, J. Phys. Chem. B, 106 (2002) 11622-11627.
[14] M. Islam, J.E. Padilla, N. Domínguez, D.C. Alvarado, M. Alam, P. Cooke, M.M.J. Tecklenburg, J.C. Noveron, Green synthesis of gold nanoparticles reduced and stabilized by squaric acid and supported on cellulose fibers for the catalytic reduction of 4-nitrophenol in water, RSC Adv., 6 (2016) 91185-91191.
[15] C.Y. Chiu, H. Wu, Z. Yao, F. Zhou, H. Zhang, V. Ozolins, Y. Huang, Facet-selective adsorption on noble metal crystals guided by electrostatic potential surfaces of aromatic molecules, J. Am. Chem. Soc., 135 (2013) 15489-15500.
[16] C.M. Mani, T. Berthold, N. Fechler, "Cubism" on the nanoscale: from squaric acid to porous carbon cubes, Small, 12 (2016) 2906-2912.
[17] T. Kikuchi, T. Yamamoto, S. Natsui, R.O. Suzuki, Fabrication of anodic porous alumina by squaric acid anodizing, Electrochim. Acta, 123 (2014) 14-22.
[18] S. Tao, T.W. Jia, Y. Yang, L.Q. Chu, BSA-sugar conjugates as ideal building blocks for SPR-based glycan biosensors, ACS Sens., 2 (2017) 57-60.

[19] W. Lai, D. Tang, L. Fu, X. Que, J. Zhuang, G. Chen, A squaric acid-stimulated electrocatalytic reaction for sensing biomolecules with cycling signal amplification, Chem.Commun., 49 (2013) 4761-4763.
[20] G. Farnia, G. Sandona, F. Marcuzzi, Electrochemical behavior of 1,2-dihydroxycyclobuten-3,4-dione in dimethyl formamide, J. Electroanal. Chem., 348 (1993) 339-354.
[21] G. Farnia, B. Lunelli, F. Marcuzzi, G. Sandona, Dicyanomethylene derivatives of squaric acid: electrochemical behavior and ESR investigation, J. Electroanal. Chem., 404 (1996) 261-269.
[22] D. Sazou, G. Kokkinidis, Electrochemical oxidation of squaric and croconic acids on platinum and platinum surfaces modified by underpotential heavy metal monolayers in acid solutions, Can. J. Chem. , 65 (1987) 397-403.
[23] R. Albalat, J. Claret, J.M. Orts, J.M. Feliu, Electrochemical behavior of squaric acid on single-crystal platinum electrodes with basal orientations in aqueous sulfuric acid medium, J. Electroanal. Chem., 334 (1992) 291-307.
[24] A. Rodes, J.M. Pérez, J.M. Orts, J.M. Feliu, A. Aldaz, FTIR study of the electrochemical behavior of squaric acid on polycrystalline platinum electrodes in 0.5M sulfuric acid, J. Electroanal. Chem., 352 (1993) 345-352.
[25] J.M. Orts, A. Rodes, R. Carbó, R. Albalat, J. Claret, Electrochemical behavior of oxocarbons on single crystal platinum electrodes Part II . Croconic acid oxidation on Pt(S)-[n(100)x(111)] surfaces in 0.5 M sulfuric acid medium, J. Electroanal. Chem., 376 (1994) 101-108.
[26] R. Carbó, R. Albalat, J. Claret, J.M. Orts, A. Rodes, J.M. Pérez, Electrochemical behaviour of oxocarbons on single crystal platinum ele ctrodes .3. Croconic acid oxidation on Pt(111) surfaces in acid medium, J. Electroanal. Chem., 404 (1996) 161-169.
[27] R. Carbó, R. Albalat, J. Claret, J.M. Orts, A. Rodes, Electrochemical behaviour of oxocarbons on single crystal platinum ele ctrodes .4. Rhodizonic acid in 0.5 M sulphuric acid medium, J. Electroanal. Chem., 424 (1997) 185-196.
[28] A. Rodes, J.M. Orts, J.M. Pérez, J.M. Feliu, A. Aldaz, On the electrochemical behavior of squaric acid on Pt(hkl) electrodes in acid solutions: a voltammetric and in situ FTIRS study, J. Electroanal. Chem., 421 (1997) 195-204.
[29] R. Carbó, R. Albalat, J. Claret, Electrochemical behaviour of oxocarbons on single crystal platinum ele ctrodes - Part V. Tetrahydroxy-p-benzoquinone in 0.5 M sulphuric acid medium, J. Electroanal. Chem., 440 (1997) 57-64.
[30] R. Carbó, R. Albalat, J. Claret, Surface cleavage of oxocarbons to CO adspecies on Pt(111) electrodes induced by metal adatoms, J. Electroanal. Chem., 449 (1998) 193-208.
[31] S. Pronkin, T. Wandlowski, ATR-SEIRAS - An approach to probe the reactivity of Pd-modified quasi-single crystal gold film electrodes, Surf. Sci., 573 (2004) 109-127.
[32] S.G. Sun, W.B. Cai, L.J. Wan, M. Osawa, Infrared absorption enhancement for CO adsorbed on Au films in perchloric acid solutions and effects of surface structure studied by cyclic voltammetry, Scanning Tunneling Microscopy, and Surface-Enhanced IR Spectroscopy, J. Phys. Chem. B, 103 (1999) 2460-2466.
[33] A.C. Sant'Ana, P.S. Santos, M.L.A. Temperini, The adsorption of squaric acid and its derived species on silver and gold surfaces studied by SERS, J. Electroanal. Chem., 571 (2004) 247-254.
[34] J. Clavilier, D. Armand, S.G. Sun, M. Petit, Electrochemical adsorption behaviour of platinum stepped surfaces in sulphuric acid solutions, J. Electroanal. Chem. , 205 (1986) 267-277.
[35] A. Rodes, E. Herrero, J.M. Feliu, A. Aldaz, Structure sensitivity of irreversibly adsorbed tin on gold single-crystal electrodes in acid media, J.Chem.Soc.Faraday.Trans., 92 (1996) 3769-3776.
[36] V. Climent, J.M. Feliu, Thirty years of platinum single crystal Electrochemistry, J.Solid State Electrochem., 15 (2011) 1297-1315.
[37] A. Hamelin, Cyclic voltammetry at gold single-crystal surfaces .1. Behaviour at low index faces, J. Electroanal. Chem., 407 (1996) 1-11.

[38] D.M. Kolb, Reconstruction phenomena at metal-electrolyte interfaces, Prog. Surf. Sci., 51 (1996) 109-173.
[39] C.D. Silva, G. Cabello, W.A. Christinelli, E.C. Pereira, A. Cuesta, Simultaneous time-resolved ATR-SEIRAS and CO-charge displacement experiments: The dynamics of CO adsorption on polycrystalline Pt, J. Electroanal. Chem., 800 (2017) 25-31.
[40] A. Rodes, J.M. Pérez, A. Aldaz, Vibrational Spectroscopy, in: W. Vielstich, H.A. Gasteiger, A. Lamm (Eds.) Handbook of Fuel Cells. Fundamentals, Technology and Applications., John Wiley & Sons Ltd., Chichester, 2003, pp. 191-219.
[41] J.M. Delgado, J.M. Orts, A. Rodes, ATR-SEIRAS study of the adsorption of acetate anions at chemically deposited silver thin film electrodes, Langmuir, 21 (2005) 8809-8816.
[42] G. Kresse, J. Hafner, Ab initio molecular dynamics of liquid metals, Phys.Rev.B, 47 (1993) 558-561.
[43] G. Kresse, J. Hafner, Ab initio molecular-dynamics simulation of the liquid-metal-amorphous-semiconductor transition in germanium, Phys.Rev.B, 49 (1994) 14251-14269.
[44] A. Eichler, J. Hafner, G. Kresse, J. Furthmuller, Relaxation and electronic surface states of rhodium surfaces, Surf. Sci., 352 (1996) 689-692.
[45] G. Kresse, J. Furthmuller, Efficiency of ab-initio total energy calculations for metals and semiconductors using a plane-wave basis set, Comput.Mater.Sci., 6 (1996) 15-50.
[46] P.E. Bloechl, Projector Augmented-Wave method, Phys.Rev.B, 50 (1994) 17953-17979.
[47] G. Kresse, D. Joubert, From ultrasoft pseudopotentials to the projector augmented-wave method, Phys.Rev.B: Condens.Matter Mater.Phys., 59 (1999) 1758-1775.
[48] J.P. Perdew, K. Burke, M. Ernzerhof, Generalized gradient approximation made simple, Phys.Rev.Lett., 77 (1996) 3865-3868.
[49] J.P. Perdew, K. Burke, M. Ernzerhof, Generalized gradient approximation made simple. [Erratum to document cited in CA126:51093], Phys.Rev.Lett., 78 (1997) 1396.
[50] M. Methfessel, A.T. Paxton, High-precision sampling for Brillouin-zone integration in metals, Phys.Rev.B: Condens.Matter, 40 (1989) 3616-3621.
[51] H.J. Monkhorst, J.D. Pack, Special points for Brillouin-zone integrations, Phys. Rev. B, 13 (1976) 5188-5192.
[52] Jmol: an open-source Java viewer for chemical structures in 3D, in, http://www. jmol. org, 2015.
[53] A. Couto, A. Rincón, M.C. Pérez, C. Gutiérrez, Adsorption and electrooxidation of carbon monoxide on polycrystalline platinum at pH 0.3-13, Electrochim. Acta, 46 (2001) 1285-1296.
[54] E. Santos, E.P.M. Leiva, W. Vielstich, U. Linke, Comparative study of carbon monoxide absorbates for different structures of platinum surfaces, J.Electroanal.Chem., 227 (1987) 199-211.
[55] J.M. Feliu, J.M. Orts, A. Fernández-Vega, A. Aldaz, J. Clavilier, Electrochemical studies in sulfuric acid solutions of adsorbed carbon monoxide on platinum (111) electrodes, J. Electroanal. Chem., 296 (1990) 191-201.
[56] J.M. Orts, A. Fernández-Vega, J.M. Feliu, A. Aldaz, J. Clavilier, Electrochemical behavior of carbon monoxide layers formed by solution dosing at open circuit on platinum(111). Voltammetric determination of carbon monoxide coverages at full hydrogen adsorption blocking in various acid media, J. Electroanal. Chem., 327 (1992) 261-278.
[57] T. Wandlowski, K. Ataka, S. Pronkin, D. Diesing, Surface enhanced infrared spectroscopy-Au(111-20 nm)/sulphuric acid - new aspects and challenges, Electrochim. Acta, 49 (2004) 1233-1247.
[58] W. Cheuquepán, A. Rodes, J.M. Orts, J.M. Feliu, Spectroelectrochemical detection of specifically adsorbed cyanurate anions at gold electrodes with (111) orientation in contact with cyanate and cyanuric acid neutral solutions, J. Electroanal. Chem., 800 (2017) 167-175.
[59] M. Osawa, Dynamic processes in electrochemical reactions studied by Surface-Enhanced InfraRed Absorption Spectroscopy (SEIRAS), Bull.Chem.Soc.Jpn., 70 (1997) 2861-2880.

[60] R.F. Aroca, D.J. Ross, C. Domingo, Surface-Enhanced Infrared Spectroscopy, Appl. Spectrosc., 58 (2004) 324A-338A.
[61] F. Kitamura, M. Takeda, M. Takahashi, M. Ito, Carbon monoxide adsorption on platinum(111) and platinum(100) single crystal surfaces in aqueous solutions studied by Infrared Reflection-Absorption Spectroscopy, Chem. Phys. Lett., 142 (1987) 318-322.
[62] S.C. Chang, M.J. Weaver, Coverage and potential-dependent binding geometries of carbon monoxide at ordered low-index platinum and rhodium-aqueous interfaces: comparisons with adsorption in corresponding metal-vacuum environments, Surf. Sci., 238 (1990) 142-162.
[63] K. Ataka, T. Yotsuyanagi, M. Osawa, Potential-dependent reorientation of water molecules at an electrode/electrolyte interface studied by Surface-Enhanced Infrared Absorption Spectroscopy, J. Phys. Chem., 100 (1996) 10664-10672.
[64] A. Berná , A. Rodes, J.M. Feliu, F. Illas, A. Gil, A. Clotet, J.M. Ricart, Structural and spectroelectrochemical study of carbonate and bicarbonate adsorbed on Pt(111) and Pd/Pt(111) electrodes, J. Phys. Chem. B, 108 (2004) 17928-17939.
[65] A. Berná, A. Rodes, J.M. Feliu, In-situ FTIR studies on the acid-base equilibria of adsorbed species on well-defined metal electrode surfaces, in: P.A. Christensen, A. Wieckowski, S.G. Sun (Eds.) In-situ Spectroscopic Studies of Adsorption at the Electrode and Electrocatalysis, Elsevier, Amsterdam, 2007, pp. 1-32.
[66] A. Berná , J.M. Delgado, J.M. Orts, A. Rodes, J.M. Feliu, In-Situ Infrared study of the adsorption and oxidation of oxalic acid at single-crystal and thin-film gold electrodes: a combined external reflection Infrared and ATR-SEIRAS approach, Langmuir, 22 (2006) 7192-7202.
[67] D.R. Lide, Ed, CRC Handbook of Chemistry and Physics, 89th Edition, CRC Press, Boca Raton, FL, 2008.
[68] M. Osawa, K. Ataka, K. Yoshii, Y. Nishikawa, Surface-enhanced Infrared Spectroscopy : the origin of the absorption enhancement and band selection rule in the infrared spectra of molecules adsorbed on fine metal particles, Appl. Spectrosc., 47 (1993) 1497-1502.
[69] A. Rodes, E. Pastor, T. Iwasita, An FTIR study on the adsorption of acetate at the basal planes of platinum single-crystal electrodes, Journal of Electroanalytical Chemistry, 376 (1994) 109-118.
[70] A. Berna, J.M. Delgado, J.M. Orts, A. Rodes, J.M. Feliu, Spectroelectrochemical study of the adsorption of acetate anions at gold single crystal and thin-film electrodes, Electrochim. Acta, 53 (2008) 2309-2321.
[71] J.M. Delgado, A. Berna, J.M. Orts, A. Rodes, J.M. Feliu, In situ Infrared study of the adsorption and surface acid-base properties of the anions of dicarboxylic acids at gold single crystal and thin-film electrodes, Journal of Physical Chemistry C, 111 (2007) 9943-9952.
[72] A. Lachenwitzer, N. Li, J. Lipkowski, Determination of the acid dissociation constant for bisulfate adsorbed at the Pt(111) electrode by subtractively normalized interfacial Fourier transform infrared spectroscopy, Journal of Electroanalytical Chemistry, 532 (2002) 85-98.
[73] A.M. Luque, A. Cuesta, J.J. Calvente, R. Andreu, Potentiostatic infrared titration of 11-mercaptoundecanoic acid monolayers, Electrochemistry Communications, 45 (2014) 13-16.
[74] T. Iwasita, A. Rodes, E. Pastor, Vibrational spectroscopy of carbonate adsorbed on Pt(111) and Pt(110) single-crystal electrodes, J. Electroanal.Chem., 383 (1995) 181-189.

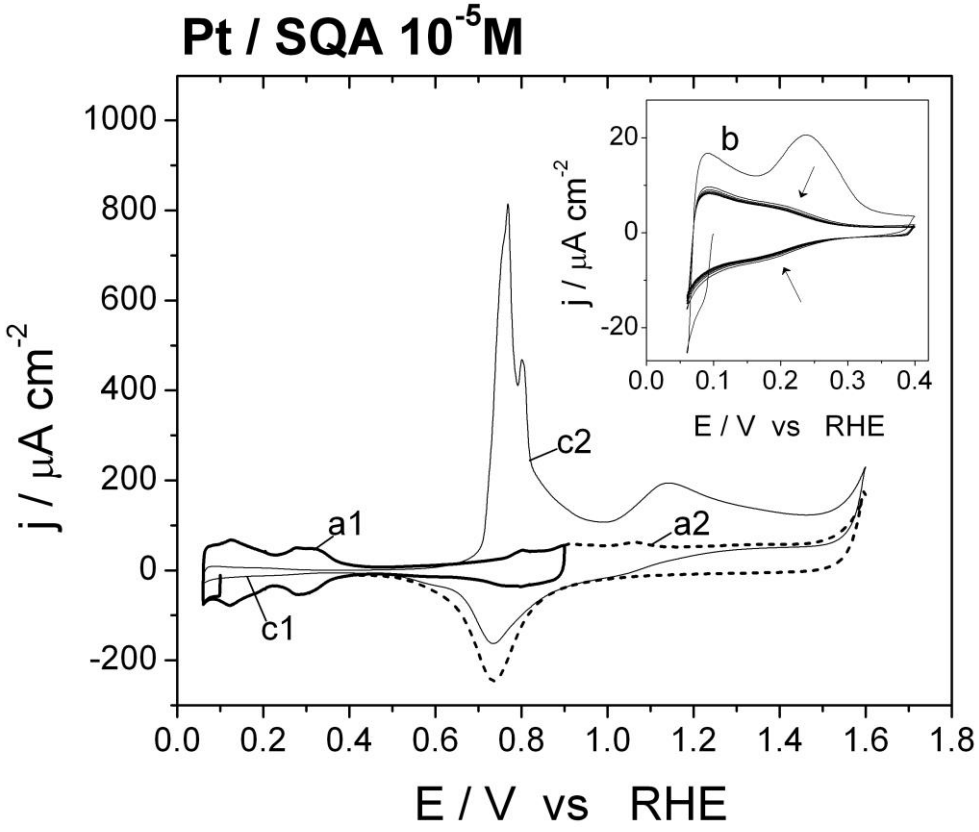

Fig. 1

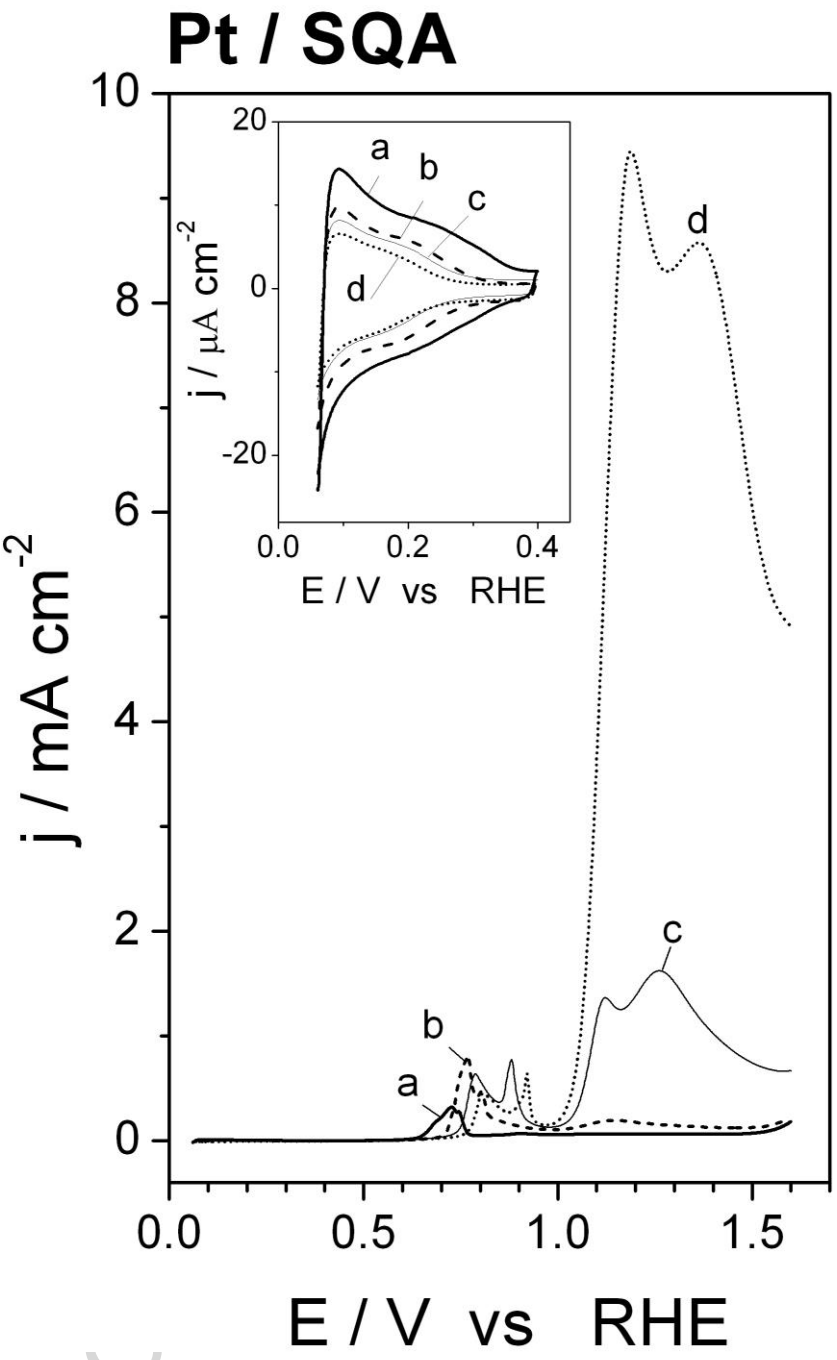

Fig. 2

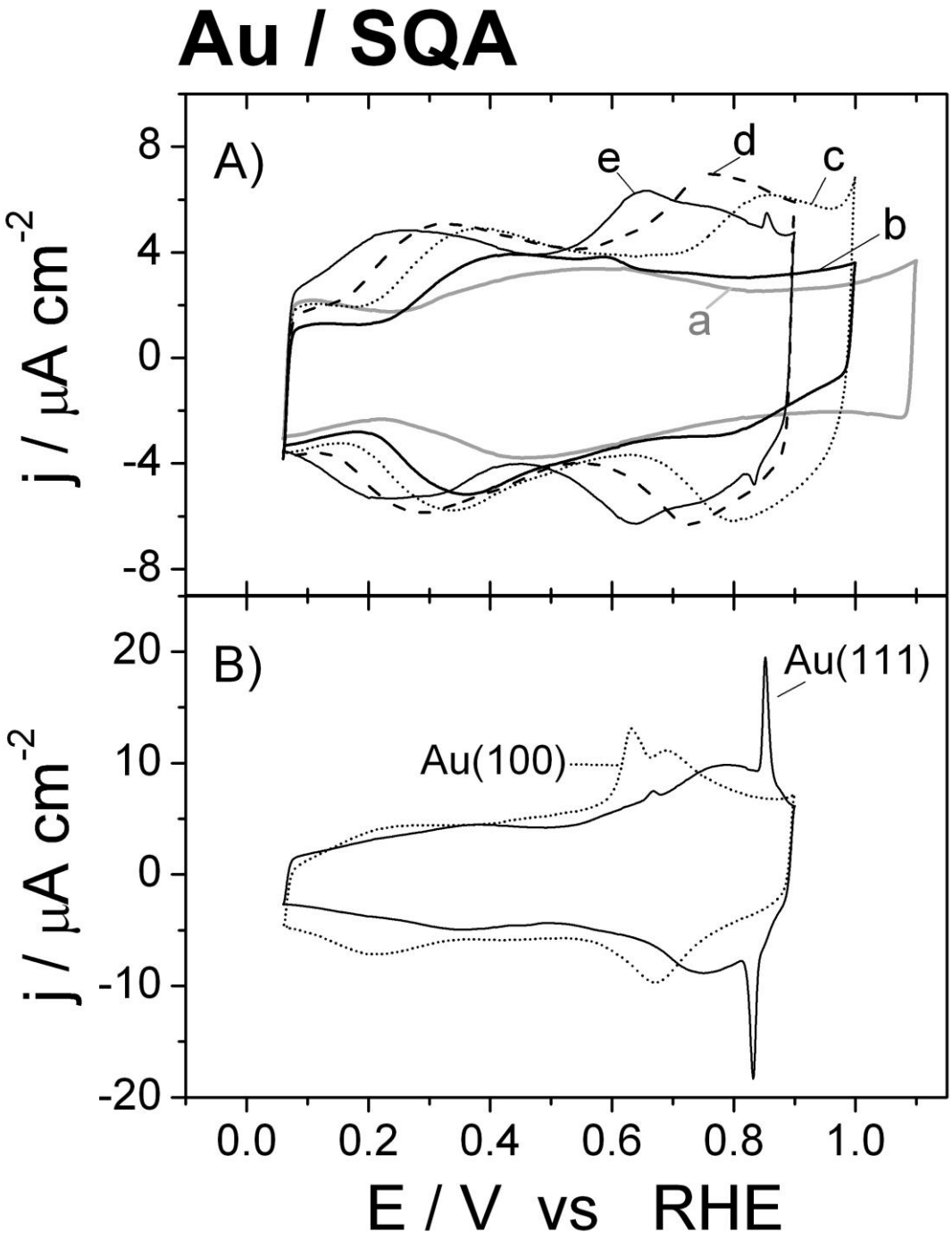

Fig. 3

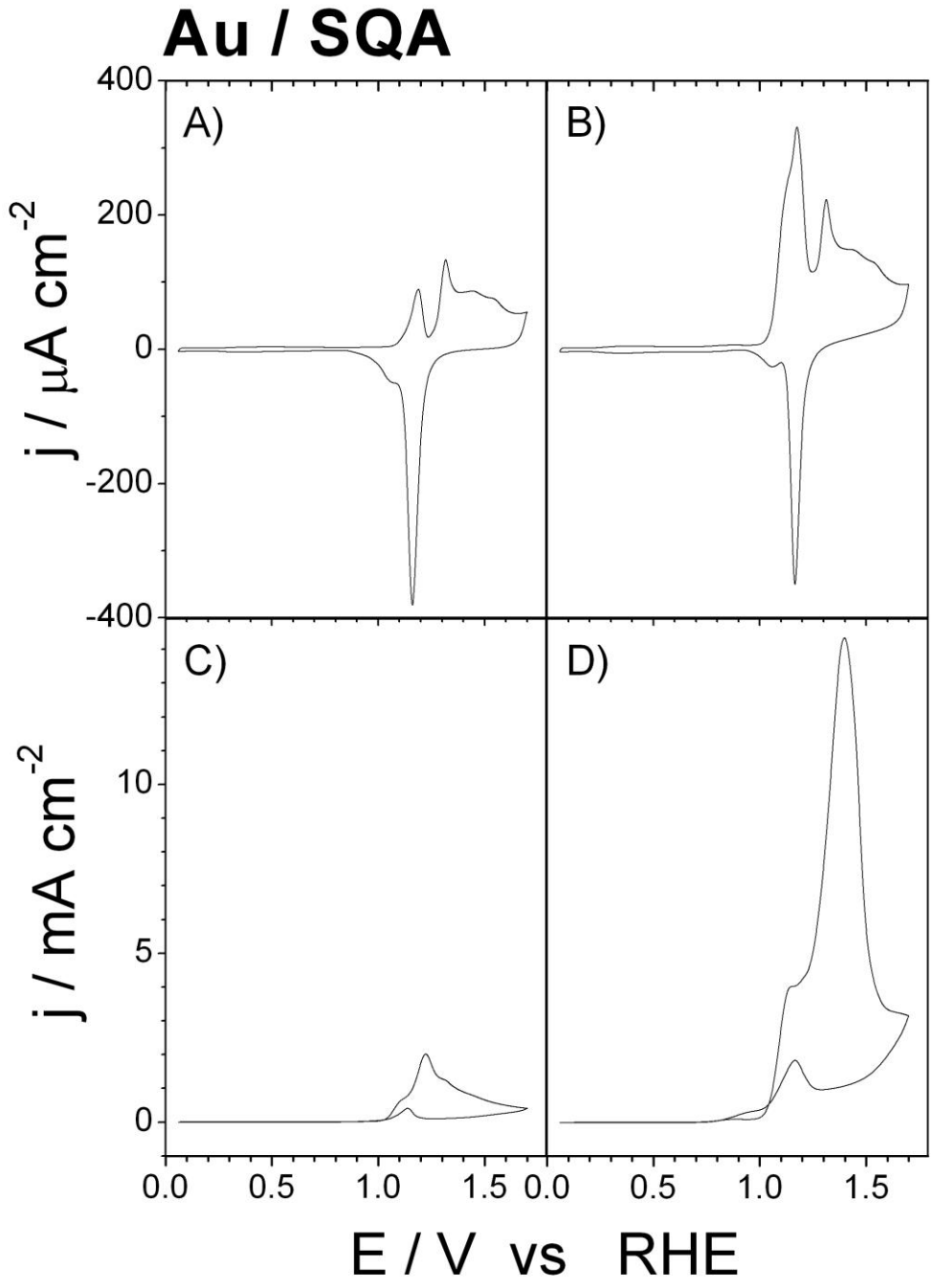

Fig. 4

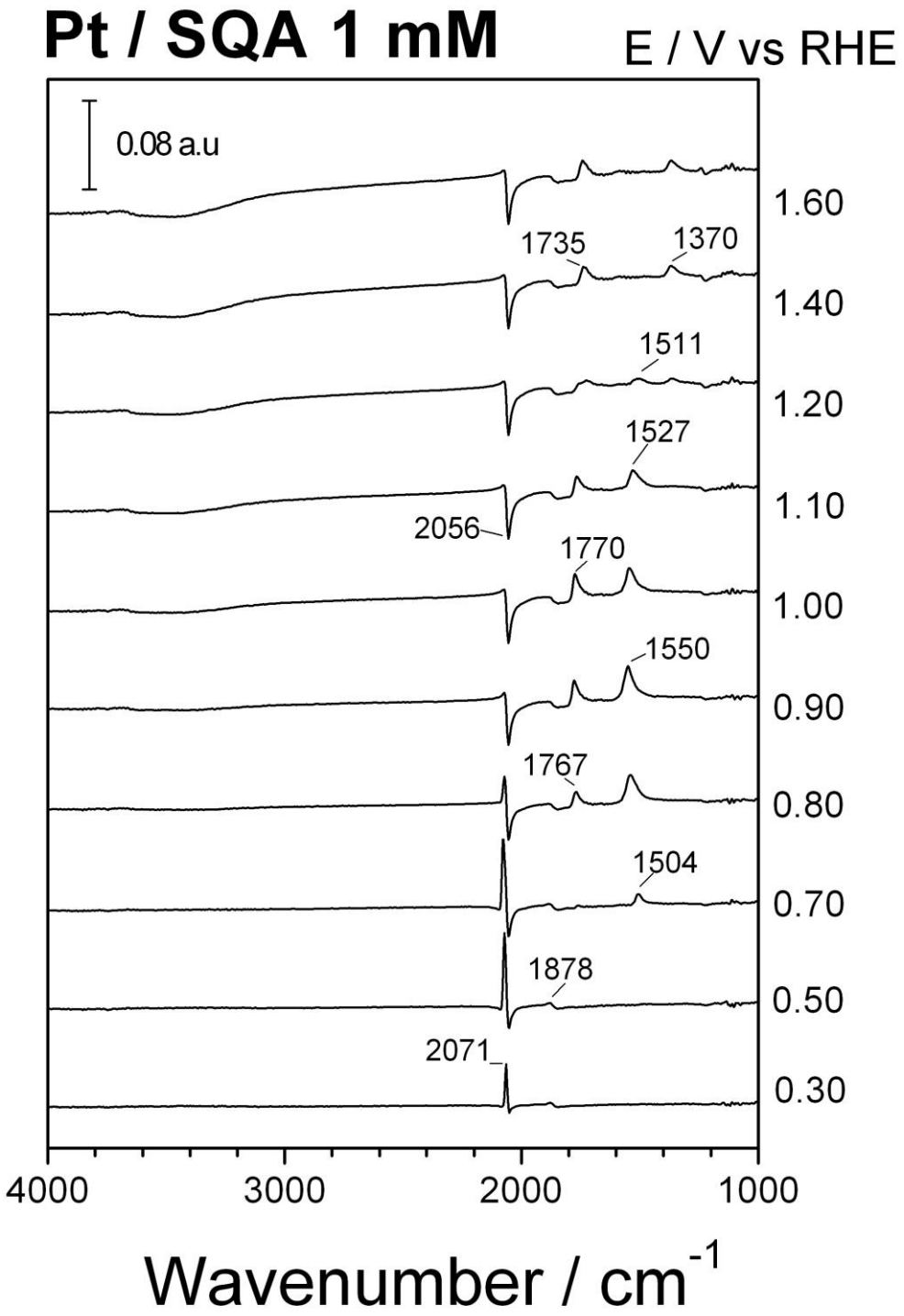

Fig. 5

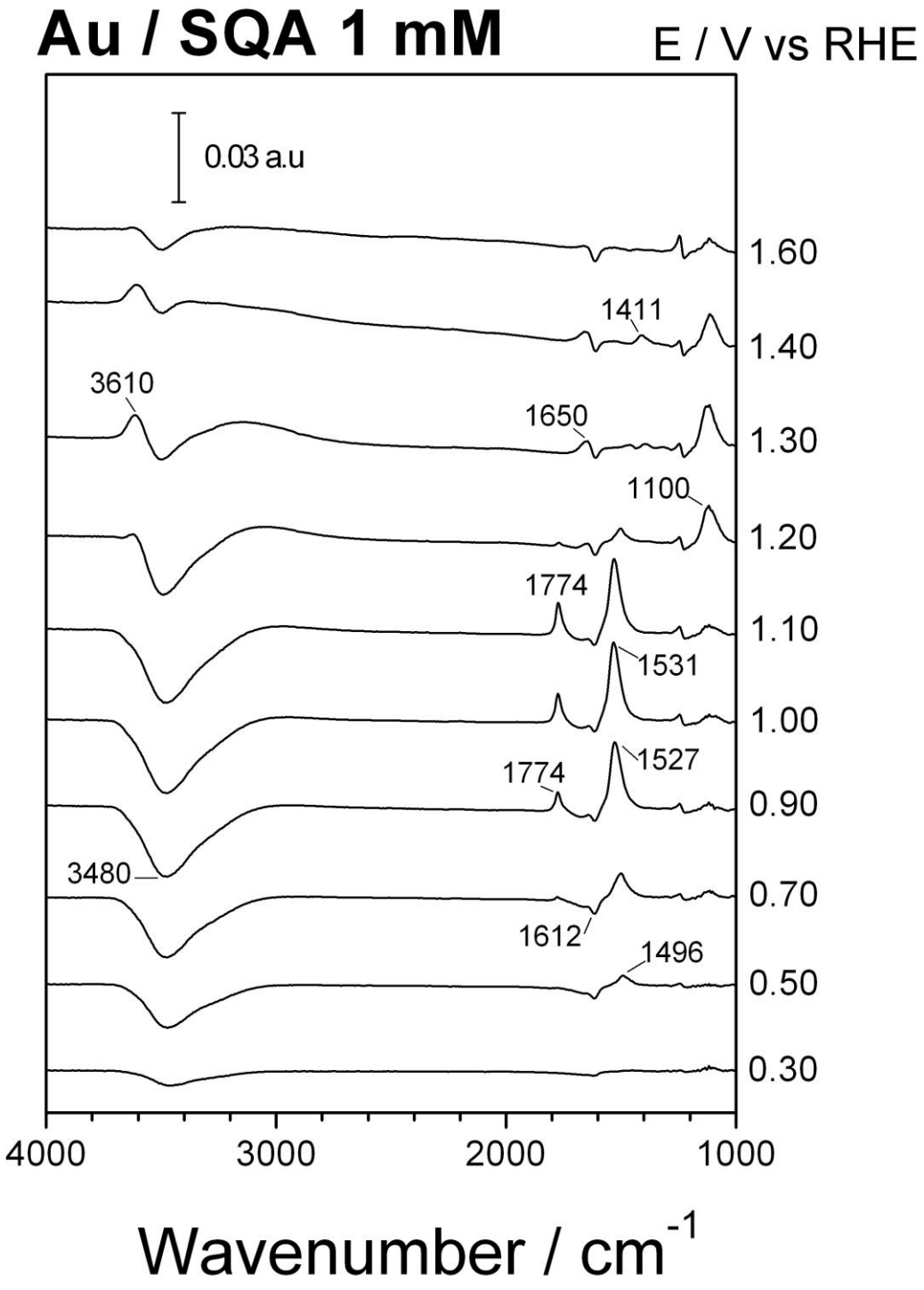

Fig. 6

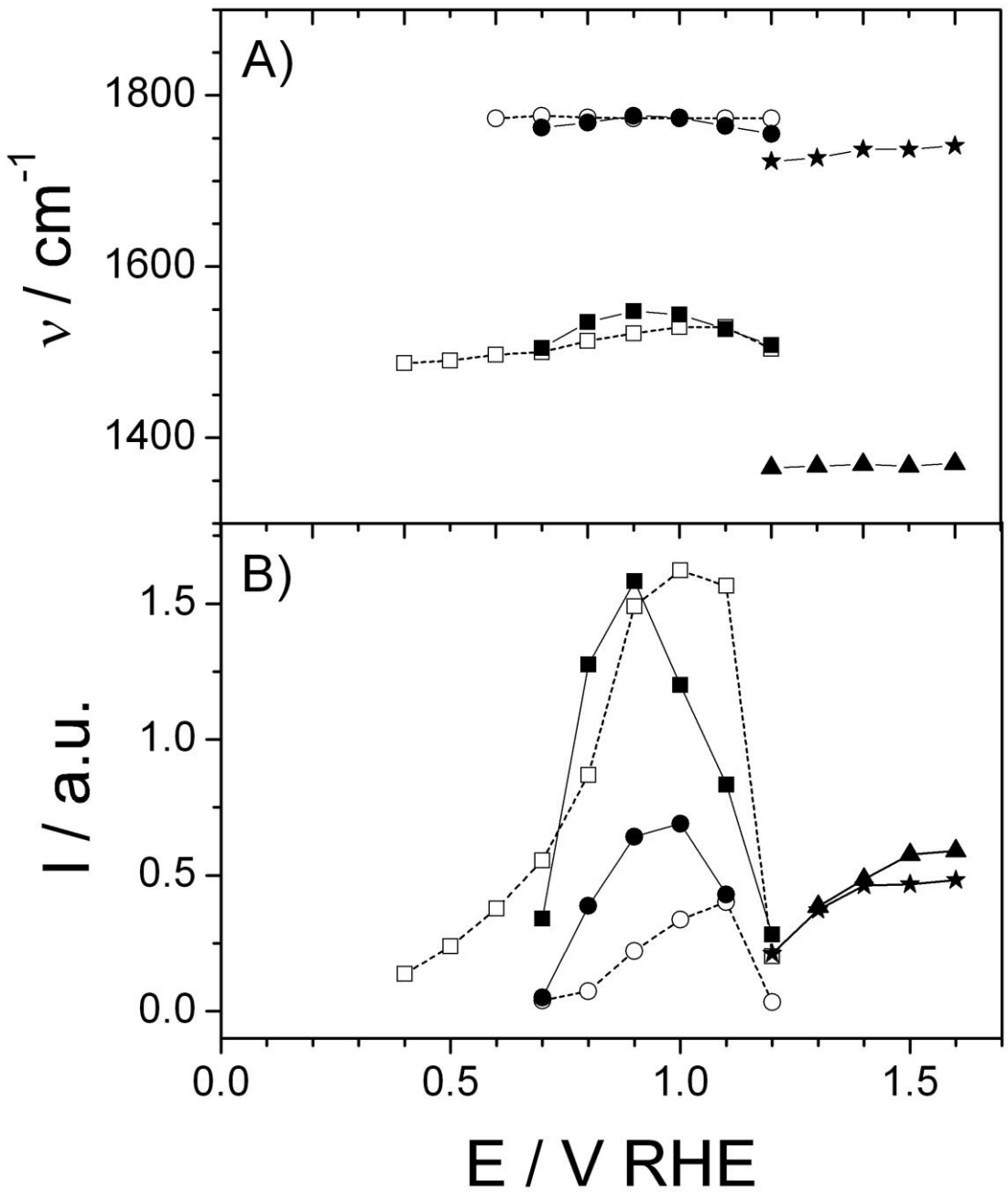

Fig. 7

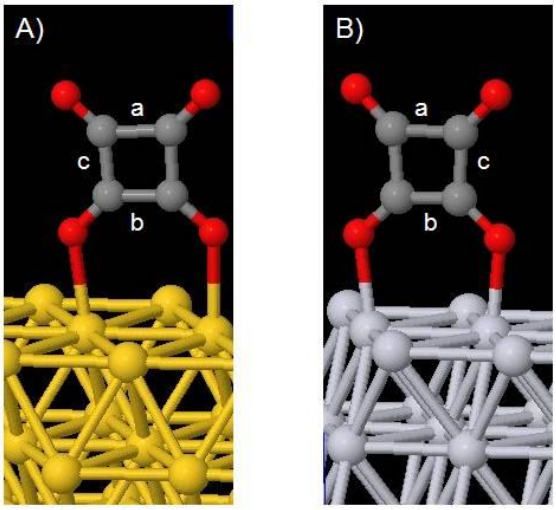

Fig. 8

Table 1. Optimized bond lenghts (in pm) for squarate (SQ) adsorbed on Au(111) and Pt(111) surfaces. The different C-C bonds (a-c) are labeled in Figure 8.

	Au(111)-SQ_{ads}	Pt(111)-SQ_{ads}
d(C-O)	121	121
d(C-O)ad	124	126
$d(C-C)_a$ (parallel, far)	156	157
$d(C-C)_b$ (parallel, close)	147	144
$d(C-C)_c$ (aprox. Normal)	151	150
d(O-metal)	239, 244	216, 217

ad: adsorbed, in direct contact with surface metal atoms.

Table 2. Calculated harmonic vibrational frequencies (in cm^{-1}) and assignments for (3x3) squarate (SQ) adlayers on Au(111) and Pt(111) surfaces. Only the main contribution to the vibrational movement is given.

Au(111)-SQ_{ads}	Pt(111)-SQ_{ads}	Assignment
1777	1780	Asym OCCO str
1768	1773	Sym OCCO str
1566	1528	Sym OadCCOad str
1530	1449	Asym OadCCOad str
1080	1098	Str C-C

ad: adsorbed, in direct contact with surface metal atoms

Highlights

1. Bidentate squarate adsorbs reversibly at Au and Pt electrodes in acidic solutions containing squaric acid (SQA).
2. Squarate adsorption at Pt is coupled to the oxidative stripping of CO formed upon dissociation of SQA.
3. Oxidation of SQA at Pt gives rise to other adsorbates probably formed upon opening of the SQA ring.